

Dynamical Casimir photons from rotation of a nonspherical particle

Guilherme C. Matos,^{1,2,*} Lucas Bianchi,^{1,†} Jeremy N. Munday,³ François Impens,¹ Reinaldo de Melo e Souza,⁴ and Paulo A. Maia Neto^{1,‡}

¹*Instituto de Física, Universidade Federal do Rio de Janeiro
Caixa Postal 68528, Rio de Janeiro, Rio de Janeiro, 21941-972, Brazil*

²*Departamento de Física, Universidade Federal de São Carlos
São Carlos, São Paulo, 13565-905, Brazil*

³*Department of Electrical and Computer Engineering,
University of California, Davis, CA 95616, USA*

⁴*Instituto de Física, Universidade Federal Fluminense, 24210-346, RJ, Brazil*

(Dated: May 29, 2026)

We consider a non-spherical neutral particle spinning in free space and interacting with the electromagnetic quantum vacuum. When the rotation axis is orthogonal to the particle symmetry axis, the scattered field develops frequency sidebands that induce the parametric emission of dynamical Casimir photon pairs. Under the structural constraint of a maximum tip velocity, the emission rate is maximized for a nearly spherical geometry and is further enhanced near a polaritonic resonance. For realistic material parameters, even these optimized upper bounds remain exceedingly small, setting stringent quantitative limits on free-space rotational dynamical Casimir emission with a single nanoparticle.

I. INTRODUCTION

Recent experiments with optically levitated dielectric nanoparticles have achieved rotation frequencies beyond the GHz range [1–6], opening a new regime of ultrafast mechanical motion. Such frequencies may enable the observation of vacuum effects associated with rotation, including rotational quantum friction near surfaces [6–9]. More broadly, the interplay between rotation and quantum vacuum physics has become a topic of growing interest, giving rise to phenomena such as quantum friction [10, 11], enhanced heat transfer [12], a quantum-vacuum analogue of the Sagnac effect [13], and nonequilibrium Casimir forces [14]. In this work, we investigate a distinct mechanism: the dynamical Casimir emission (DCE) of photon pairs generated by a spinning anisotropic particle rather than by an oscillating boundary [15–23].

The recent progress in ultrafast levitated rotation naturally raises the question of whether DCE could be observed in such experimental platforms. So far, the small magnitude of oscillation-induced DCE under realistic conditions has hindered its direct observation, although an analog realization has been demonstrated in circuit QED [24].

In the present setting, dynamical Casimir emission originates from the frequency modulation of the anisotropic scattering response induced by rotation. When the rotation axis is not a symmetry axis, sidebands couple positive- and negative-frequency field components, leading to a Bogoliubov mixing between annihilation and creation operators [25–28] and hence to photon

creation from the vacuum. The spectral range involved in this spinning-induced DCE increases with the rotation frequency Ω , resulting in a strong dependence of the emission rate on the spinning frequency. In contrast to quantum friction [11, 29–33], the mechanism considered here does not require a lossy material medium.

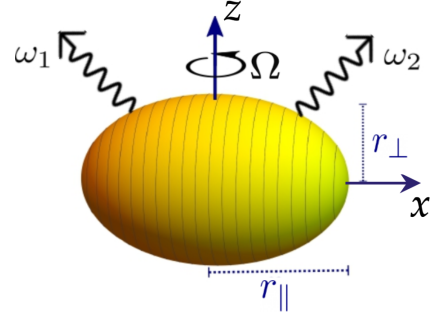


FIG. 1. Dynamical Casimir Effect (DCE) radiation from a rotating spheroid. The spheroid rotates at angular velocity Ω about the z -axis, which is orthogonal to its symmetry axis (along the x direction). The particle's anisotropic polarizability enables rotational sideband mixing of vacuum fluctuations, driving the emission of photon pairs that satisfy the condition $\omega_1 + \omega_2 = 2\Omega$.

Preliminary studies of spinning-induced DCE were carried out using a two-dimensional scalar-field toy model [18]. However, assessing the feasibility of such experiments requires a complete theory in a realistic three-dimensional setting. Here we develop such a framework, including a full treatment of the quantized electromagnetic field together with a realistic dispersive material response. We show how the emission can be enhanced by tuning the rotation frequency close to the GHz polaritonic resonance of a Barium Strontium Titanate (BST) nanoparticle [9, 34, 35]. As the simplest anisotropic ge-

* gcmatos@ufscar.br

† lucasbnchm@gmail.com

‡ pamn@if.uffj.br

ometry, we consider a spheroidal particle rotating about an axis orthogonal to its symmetry axis. We find that the eccentricity maximizing the DCE emission has a nontrivial dependence on particle size. Because the attainable rotation frequency is fundamentally limited by the maximum tip velocity supported by the material, we also derive geometry-optimized upper bounds for the DCE emission rate for a given material.

In Sec. II, we derive the emission spectrum and total photon-production rate in terms of the polarizability tensor of the rotating particle. In Sec. III, we apply the theory to BST spheroids and identify the geometric and resonant conditions that maximize the effect under realistic constraints. Section IV concludes with a discussion of the observability limits of free-space rotational dynamical Casimir emission.

II. DCE FREQUENCY SPECTRUM FOR A SPINNING PARTICLE

Here we develop the general theoretical framework for dynamical Casimir emission from a spinning nano-object and show that it depends critically on the particle anisotropy. We derive the scaling of DCE emission with the rotation frequency and compare it with known DCE results: Ω^5 for an oscillating plane mirror of large transverse size [27, 36, 37], and Ω^9 for subwavelength mirrors [38], oscillating spherical particles [39], and oscillating ground-state atoms [40].

A. Input-output transformation in the dipolar regime

Within the dipole approximation, the scattering by a rotating nanoparticle (located at the origin) yields the following input-output relation for the electric field [27]:

$$\mathbf{E}_{\text{out}}(\mathbf{r}, \omega) = \mathbf{G}(\mathbf{r}, \mathbf{r}' = 0, \omega) \cdot \mathbf{d}(\omega) + \mathbf{E}_{\text{in}}(\mathbf{r}, \omega), \quad (1)$$

where $\mathbf{d}(\omega)$ is the particle's induced electric dipole while $\mathbf{G} = \mathbf{G}^R - \mathbf{G}^A$ is the difference between the retarded and advanced Green's functions. In the radiation zone, the latter is given by

$$\mathbf{G}(\mathbf{r}, \mathbf{r}' = 0, \omega) = \frac{2i\omega^2 \sin\left(\frac{\omega r}{c}\right)}{4\pi\epsilon_0 c^2 r} \left[\mathbb{1} - \frac{\mathbf{r} \otimes \mathbf{r}}{r^2} \right]. \quad (2)$$

For a localized scatterer, it is convenient to expand the input and output fields as a sum over multipolar spherical waves [41, 42]:

$$\mathbf{E}_{\text{in}}(\mathbf{r}, \omega) = i\mathcal{E}(\omega) \sum_{jm\lambda} \left[a_{jm\lambda}^{\text{in}}(\omega) \Theta(\omega) \mathbf{I}_{jm\lambda}(\mathbf{r}, \omega) - a_{jm\lambda}^{\text{in}\dagger}(-\omega) \Theta(-\omega) \mathbf{I}_{jm\lambda}^*(\mathbf{r}, \omega) \right], \quad (3)$$

and likewise for the output field $\mathbf{E}_{\text{out}}(\mathbf{r}, \omega)$, where Θ denotes the Heaviside step function and $\mathcal{E}(\omega) = \sqrt{\frac{\hbar\omega}{2\epsilon_0 c}}$.

Here, $j = 1, 2, \dots$ denotes the multipole order (equivalently, the total angular-momentum quantum number), while $m = -j, \dots, j$ corresponds to its projection along the z axis. The spherical-wave modes $\mathbf{I}_{jm\lambda}(\mathbf{r}, \omega)$ [42] are labeled by $\lambda = \text{E, M}$, corresponding to electric and magnetic multipoles respectively. In the radiation zone, the electric multipole modes can be approximated by:

$$\mathbf{I}_{jm\text{E}}(\mathbf{r}, \omega) \approx \frac{4\pi i^{j-1}}{\sqrt{j(j+1)}} \frac{\cos\left(\frac{\omega r}{c} - \frac{j\pi}{2}\right)}{r} \nabla Y_{jm}(\hat{\mathbf{r}}), \quad (4)$$

where $Y_{jm}(\hat{\mathbf{r}})$ denote the spherical harmonics. The operators $a_{jm\lambda}^{\text{in}}(\omega)$ and $a_{jm\lambda}^{\text{in}\dagger}(\omega)$ of the quantized light field obey the standard commutation relations.

We derive a Bogoliubov transformation between input and output bosonic operators, mediated by the dipole moment of the spinning particle, by replacing the expansion (3) into (1) and taking the asymptotic expressions (2) and (4) into account. As expected from selection rules, only the electric dipole modes ($j = 1; m = 0, \pm 1, \text{E}$) are excited:

$$\begin{aligned} a_{10\text{E}}^{\text{out}}(\omega) &= \frac{\omega^2}{2\sqrt{6}\pi^{3/2}\epsilon_0 c^2 \mathcal{E}(\omega)} d_z(\omega) + a_{10\text{E}}^{\text{in}}(\omega) \\ a_{1\pm 1\text{E}}^{\text{out}}(\omega) &= \frac{\mp \omega^2}{4\sqrt{3}\pi^{3/2}\epsilon_0 c^2 \mathcal{E}(\omega)} (d_x(\omega) \mp i d_y(\omega)) \\ &\quad + a_{1\pm 1\text{E}}^{\text{in}}(\omega) \end{aligned} \quad (5)$$

B. Spectrum and total emission rate

The number of photons emitted into mode ($j = 1, m, \text{E}$) within the frequency interval $[\omega, \omega + d\omega]$, per interaction time T , is

$$d\Gamma_m = \frac{1}{T} \langle 0_{\text{in}} | a_{1m\text{E}}^{\text{out}\dagger}(\omega) a_{1m\text{E}}^{\text{out}}(\omega) | 0_{\text{in}} \rangle d\omega. \quad (6)$$

The corresponding spectra of emission are given by

$$\frac{d\Gamma_0}{d\omega} = \frac{1}{12\pi^3} \frac{\omega^3}{\hbar c^3 \epsilon_0} C_{zz}(\omega) \quad (7)$$

$$\frac{d\Gamma_{\pm 1}}{d\omega} = \frac{1}{48\pi^3} \frac{\omega^3}{\hbar c^3 \epsilon_0} [C_{xx}(\omega) + C_{yy}(\omega) \pm i(C_{yx}(\omega) - C_{xy}(\omega))], \quad (8)$$

where

$$C_{\mu\nu}(\omega) = \langle 0_{\text{in}} | d_\mu^\dagger(\omega) d_\nu(\omega) | 0_{\text{in}} \rangle \quad (9)$$

are the elements of the dipole correlation matrix (μ, ν denoting Cartesian components).

We now consider a nanoparticle rotating with angular frequency Ω about the z axis, orthogonal to the symmetry axis taken along x (Fig. 1). The induced dipole of the particle at rest is $\mathbf{d}_{\text{rest}}(\omega) = \boldsymbol{\alpha}_{\text{rest}}(\omega) \cdot \mathbf{E}(0, \omega)$, with the polarizability tensor

$$\boldsymbol{\alpha}_{\text{rest}}(\omega) = \begin{pmatrix} \alpha_{\parallel}(\omega) & 0 & 0 \\ 0 & \alpha_{\perp}(\omega) & 0 \\ 0 & 0 & \alpha_{\perp}(\omega) \end{pmatrix}. \quad (10)$$

Rotation modulates the polarizability and generates sidebands at frequencies $\omega \pm 2\Omega$, because a full modulation cycle corresponds to a half turn of the particle. Under these conditions, the induced electric dipole is given by (see Appendix A)

$$\mathbf{d}(\omega) = \boldsymbol{\alpha}_0(\omega) \cdot \mathbf{E}_{\text{in}}(\mathbf{0}, \omega) + \sum_{\sigma=\pm} \boldsymbol{\alpha}_\sigma(\omega) \cdot \mathbf{E}_{\text{in}}(\mathbf{0}, \omega + 2\sigma\Omega). \quad (11)$$

The dipole correlation matrix $C_{\mu\nu}(\omega)$ is obtained from Eqs. (9) and (11). Owing to the vacuum expectation value (9), it involves only correlations between red- and blue-detuned sideband components of the dipole, associated with frequency shifts $\omega \mp 2\Omega$. Thus, the polarizability tensor $\boldsymbol{\alpha}_0(\omega)$ capturing the dipole response at the electric field frequency is irrelevant for DCE. By contrast, the sideband generation and DCE emission depends crucially on the Doppler-shifted susceptibility tensors

$$\boldsymbol{\alpha}_\pm(\omega) = \frac{\Delta(\omega \pm \Omega)}{2} \begin{pmatrix} 1 & \mp i & 0 \\ \mp i & -1 & 0 \\ 0 & 0 & 0 \end{pmatrix} \quad (12)$$

which scale with the geometry-dependent anisotropic response

$$\Delta(\omega) = \frac{\alpha_{\parallel}(\omega) - \alpha_{\perp}(\omega)}{2}. \quad (13)$$

In particular, $\boldsymbol{\alpha}_\pm(\omega)$ vanish if the particle response is isotropic in the plane perpendicular to the rotation axis, suppressing Bogoliubov mixing in this case. While a rotating isotropic nanoparticle may exhibit other rotation-induced effects [10, 13, 14, 29], anisotropy in the plane orthogonal to the rotation axis is a necessary condition for spinning-induced DCE.

As expected, $d_z(\omega)$ is unaffected by rotation about the z axis. This reflects a selection rule, since $\boldsymbol{\alpha}_\pm$ couple only the x and y components [Eq. (12)] – modes with $m = 0$ do not contribute to the emission. In addition, radiation in the $m = -1$ channel vanishes in Eq. (8) by destructive quantum interferences. Hence, DCE radiation occurs only into the mode $m = 1$, so that $d\Gamma \equiv d\Gamma_1$. The emission spectrum is given by:

$$\frac{d\Gamma}{d\omega} = \frac{|\omega - 2\Omega|^3 \omega^3 |\Delta(\omega - \Omega)|^2 \Theta(2\Omega - \omega)}{36\pi^3 c^6 \epsilon_0^2}. \quad (14)$$

The DCE spectrum is confined to the range $[0, 2\Omega]$, where rotational modulation generates a negative-frequency sideband that enables Bogoliubov mixing. Furthermore, the invariance of Eq. (14) under $\omega \rightarrow 2\Omega - \omega$ shows that the spectrum is mirror-symmetric about the midpoint $\omega = \Omega$. This is indeed a fundamental property of DCE, which emits photons in pairs with frequencies satisfying $\omega_1 + \omega_2 = 2\Omega$ [15, 27, 40].

The total emission rate is obtained by integrating the emission spectrum (14) over all frequencies:

$$\Gamma(\Omega) = \frac{1}{144\pi^3 c^6 \epsilon_0^2} \int_0^{2\Omega} d\omega \omega^3 |\omega - 2\Omega|^3 |\Delta(\omega - \Omega)|^2. \quad (15)$$

Equations (14) and (15) constitute the central results of this work. They show that the core ingredient for rotational DCE is the anisotropy function $\Delta(\omega)$, which encodes the shape-induced difference between the parallel and transverse polarizabilities. Those polarizabilities are determined by the dielectric function $\epsilon(\omega)$ of the particle's material. For most dielectric materials, the resonant frequencies are all much higher than the rotation frequency Ω , allowing us to neglect dispersion and approximate $\Delta(\omega)$ by its zero-frequency value over the spectral range limited by 2Ω in (15). The emission rate can then be approximated by its quasi-static limit

$$\Gamma_{\text{qs}} = \frac{2}{315\pi^3 c^6 \epsilon_0^2} |\Delta(0)|^2 \Omega^7. \quad (16)$$

As shown below, for the GHz rotation frequencies achieved with optically levitated SiO_2 nanodumbbells [1–4], the quasi-static regime applies and yields an extremely weak DCE emission. To circumvent this limitation, we investigate materials with polaritonic resonances in the GHz range, which enable to overcome the quasi-static regime and provide an enhanced emission rate.

III. DCE RADIATION FROM A SPINNING SPHEROID

As a simple example of an anisotropic object, we consider a prolate spheroid rotating about an axis perpendicular to its symmetry axis (Fig. 1) and obtain the corresponding DCE emission rate using the general theory developed in Sec. II. We first analyze the anisotropy function for this geometry and briefly discuss the case of SiO_2 nanoparticles, then investigate resonant enhancement in a BST material, and finally optimize the nanoparticle geometry to maximize the emission at fixed tip velocity.

A. Anisotropy function and the case of SiO_2

Using the analytical polarizability of a dielectric spheroid at rest [43], we obtain the anisotropy function $\Delta(\omega)$ governing the rotational DCE. For a prolate spheroid with radii r_{\perp} and r_{\parallel} ($r_{\parallel} > r_{\perp}$), we find

$$\Delta(\omega) = \frac{r_{\parallel} r_{\perp}^2 (N_{\parallel}^{-1} - N_{\perp}^{-1})(\epsilon(\omega) - 1)^2}{4\pi\epsilon_0 \cdot 6(\epsilon(\omega) - 1 + N_{\parallel}^{-1})(\epsilon(\omega) - 1 + N_{\perp}^{-1})}, \quad (17)$$

where $\epsilon(\omega)$ is the dielectric function of the material and N_i are the depolarizing factors, defined as functions of the eccentricity $e = \sqrt{1 - r_{\perp}^2/r_{\parallel}^2}$:

$$N_{\parallel} = \frac{1 - e^2}{2e^3} \left[\ln \left(\frac{1 + e}{1 - e} \right) - 2e \right], \quad (18)$$

$$N_{\perp} = \frac{1}{2}(1 - N_{\parallel}).$$

Because the lowest resonance frequency of SiO₂ lies in the THz range, its dielectric function can be approximated by $\epsilon(0)$ when considering (15) for the GHz rotation frequencies achieved in recent optical levitation experiments [1–5]. The emission rate is then obtained from the quasi-static limit (16) in terms of the anisotropy function at zero frequency.

As an example, we consider the parameters of the experiment reported in Ref. [3], with $\Omega/(2\pi) = 5.2$ GHz. As a crude approximation, we model the SiO₂ nanodumbbell as a prolate spheroid with semi-axes $r_{\parallel} = 2r_{\perp} = D$, where $D = 150$ nm is the diameter of the two nanospheres that are connected as a composite. By computing $\Delta(0)$ from (17)-(18) with $\epsilon(0) = 3.9$ and plugging the result into (16), we obtain the extremely small emission rate $\Gamma_{\text{qs}} = 2.5 \times 10^{-21} \text{ s}^{-1}$. Next, we show how the emission rate is enhanced by operating beyond the quasi-static regime exploiting a GHz polaritonic resonance.

B. Polaritonic-enhanced DCE from a BST nanoparticle

Materials with polaritonic resonances in the GHz range can strongly enhance the emission rate. BST provides a natural example, because its resonance frequency lies close to the highest experimentally achieved rotation frequencies [3, 4, 9]. In this subsection, we consider a BST spheroid with the same dimensions discussed in the previous paragraph.

We model the dielectric response of BST as an isotropic material using a single-resonance Lorentz function

$$\epsilon(\omega) = \epsilon_{\text{UV}} + \frac{\epsilon(0) - \epsilon_{\text{UV}}}{1 - (\omega/\omega_T)^2 + i\omega\gamma/\omega_T^2} \quad (19)$$

with experimentally-measured parameters taken from Refs. [9, 34]: resonance frequency $\omega_T = 5.7 \times 10^9$ rad/s, damping rate $\gamma = 2.8 \times 10^8$ Hz, static permittivity $\epsilon(0) = 7.1$, and high-frequency permittivity $\epsilon_{\text{UV}} = 2.896$. This single-oscillator model [Eq. (19)] is sufficiently accurate for our purposes, because we only consider frequencies ω in the GHz range, well below additional resonances that typically lie in the UV domain. The net effect of these UV resonances is nevertheless accounted for by the constant term ϵ_{UV} in Eq. (19), ensuring consistency with the expected static and high-frequency permittivities.

The quasi-static limit, corresponding to very slow rotations with $\Omega \ll \omega_T$, offers a valuable benchmark for the full theory. From Eq. (16), we obtain

$$\Gamma_{\text{qs}} = 2.0 \times 10^{-44} (\Omega[\text{GHz}])^7 \text{ s}^{-1}. \quad (20)$$

We compute the emission spectrum by combining Eqs. (14), (17), and (19). Figure 2(a) shows the spectrum for several values of Ω/ω_T and reveals a structural change as Ω exceeds the resonance frequency ω_T . For $\Omega = 0.5\omega_T$, the spectrum remains close to the smooth polynomial form of the quasi-static limit. As

Ω approaches ω_T , resonance peaks inherited from the anisotropy function $\Delta(\omega)$ emerge. These peaks become progressively narrower as Ω increases further.

Using this model, we compare the exact spectrum-integrated result for the emission rate Γ (15) with the quasi-static limit [Eqs. (16) and (20)]. Figure 2(b) shows the enhancement factor $\Gamma/\Gamma_{\text{qs}}$ versus angular velocity Ω . The resonant enhancement is clearly identified by a peak at $\Omega \sim \omega_T$. As the angular velocity increases beyond resonance, the enhancement $\Gamma/\Gamma_{\text{qs}}$ decays as $1/\Omega$, because in the high-frequency regime ($\Omega \gg \omega_T$) the emission rate scales as $\Gamma \sim \Omega^6$.

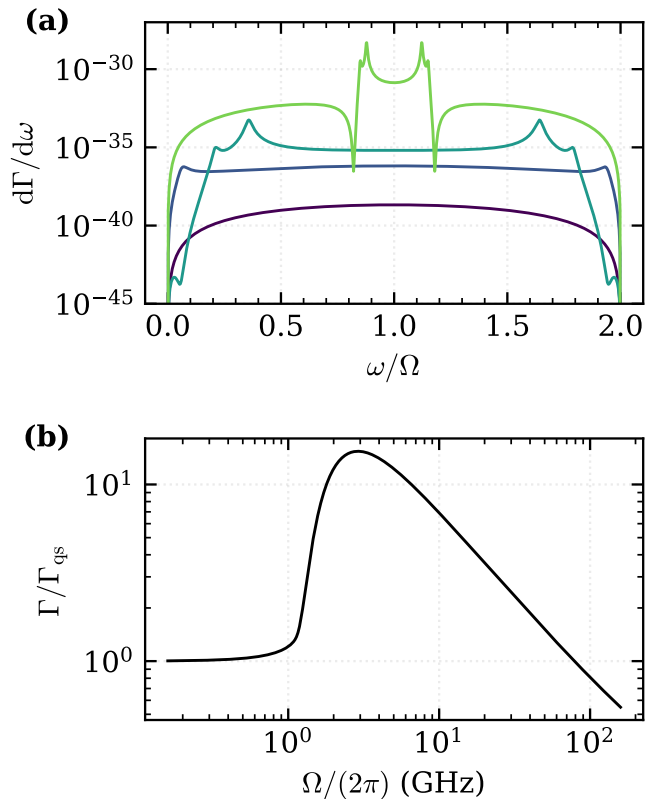


FIG. 2. DCE emission of a prolate BST spheroid rotating about an axis orthogonal to its symmetry axis. (a) Emission spectrum for (from top to bottom) $\Omega/\omega_T = 10, 1.9, 1.3, 0.5$, where $\omega_T/(2\pi) = 0.91$ GHz is the BST resonance frequency. (b) Enhancement ratio (with respect to the quasi-static limit) $\Gamma/\Gamma_{\text{qs}}$ versus rotational frequency $\Omega/(2\pi)$.

C. Optimal Geometry and Fundamental Limits under a Material Burst-Speed Constraint

We now optimize the spheroid size and shape to maximize DCE radiation, treating the spheroid eccentricity, radius and spinning frequency as free parameters. A key constraint is that the linear circumferential velocity of a spinning solid particle is bounded by the burst speed v_b characteristic of a given material [44]. In a spinning pro-

late spheroid, the fastest point is at a distance r_{\parallel} from the rotation axis, and therefore the angular velocity is restricted by $\Omega r_{\parallel} \leq v_b = \sqrt{\frac{\text{UTS}}{\rho}}$, where UTS is the ultimate tensile strength and ρ is the density.

In order to estimate an upper bound for the emission rate, we consider the UTS of carbon nanotubes, which is approximately $\sim 10^3$ higher than in the case of SiO_2 . The burst speed is then ~ 30 higher than the value achieved in Ref. [3] for SiO_2 nanoparticles, which leads to the upper bound estimation of $v_b = 1.5 \times 10^5$ m/s.

We consider the angular velocity at its limit value $\Omega = v_b/r_{\parallel}$ and plot the resulting emission rate Γ as a function of r_{\parallel} for different values of eccentricity in Fig. 3(a). The dielectric function of the material is the same as considered in the previous sub-section.

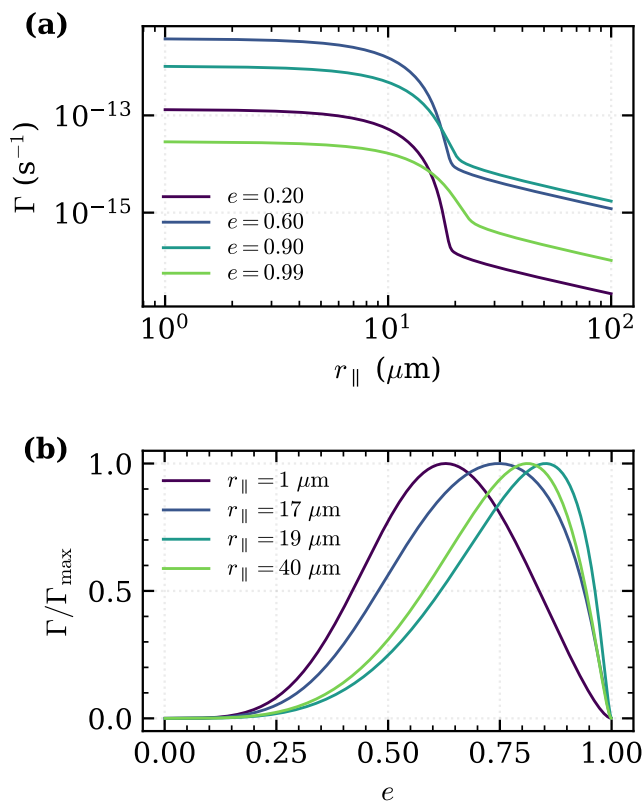


FIG. 3. DCE emission from a spheroid at fixed tip velocity $v_b = \Omega r_{\parallel} = 1.5 \times 10^5$ m/s. (a) Emission rate as a function of the major semi-axis r_{\parallel} for several eccentricities e . The crossover from the small-size limit (high frequencies) to the large-size one (low frequencies) takes place at $r_{\parallel} \sim v_b/\omega_T = 26 \mu\text{m}$. The range shown spans rotational frequencies $\Omega/(2\pi)$ from 24 GHz to 0.24 GHz. (b) Emission rate as a function of the eccentricity e for different values of r_{\parallel} . Each curve is normalized by its maximum value.

From (15) and (17), Γ scales as r_{\parallel}^6 at a fixed eccentricity. The nontrivial dependence shown in Fig. 3(b) arises from the constraint $\Omega = v_b/r_{\parallel}$. The plateau for small particles shown in Fig. 3(a) corresponds to the

high-frequency limit $\Omega \gg \omega_T$ for which $\Gamma \sim \Omega^6$ thus cancelling the dependence on r_{\parallel} for small particles.

The crossover from the high-frequency limit to the quasi-static regime takes place at $r_{\parallel} \sim 10 \mu\text{m}$. For larger particles, the frequencies are such that $\omega \ll \omega_T$ and then from (16) $\Gamma \sim r_{\parallel}^6 \Omega^7 \sim 1/r_{\parallel}$ as illustrated by Fig. 3(a). The overall conclusion is that small particles such that $r_{\parallel} < v_b/\omega_T$ lead to a higher emission rate (for a given tip linear velocity v_b). However, using smaller particles require driving the rotation at a higher frequency in order to reach the linear velocity limit underlying our calculation.

The comparison between different curves in Fig. 3(a) shows that more elongated particles tend to optimize the emission rate in the case of large particles, except for the extreme ‘needle-like’ case $e = 0.99$. On the other hand, the intermediate value $e = 0.6$ leads to the highest rate for small particles, among the examples shown in the figure.

We investigate in more detail how the particle’s shape can be optimized in Fig. 3(b), which shows the variation of the emission rate with the eccentricity for different values of r_{\parallel} . As the size increases, the optimal value is displaced towards more elongated spheroids, but when reaching the quasi-static limit [$r_{\parallel} > 20 \mu\text{m}$ according to Fig. 3(a)], such trend is slightly reversed.

IV. CONCLUSIONS

In this work, we have shown that a rapidly rotating non-spherical dielectric nanoparticle can emit photons through the dynamical Casimir effect. We developed a theory based on the scattering of the full electromagnetic field by the spinning particle, where rotation generates frequency sidebands and induces Bogoliubov mixing of field modes. The emission is governed by the spectral anisotropy of the polarizability response, which depends critically on both particle geometry and material properties.

We investigated the corresponding DCE emission in a typical setting of optically levitated SiO_2 nanoparticles spinning at GHz frequencies. This corresponds to the quasi-static regime, where emission is determined by the static anisotropy and the rotation frequency. The presence of polaritonic resonances near the rotation frequency can lift this limitation and significantly enhance the emission rate. We provide realistic estimates for BST nanospheroids, which exhibit such resonances in the GHz range.

Finally, we show that the attainable emission is fundamentally constrained by the material burst velocity, which sets a maximum angular frequency for a given nanoparticle geometry. By optimizing the geometry of BST nanospheroids under this constraint, we determine the corresponding upper bounds on the DCE emission.

Despite these enhancements, the predicted rates remain exceedingly small, thereby establishing stringent

quantitative limits on free-space rotational dynamical Casimir emission with a single particle. These results indicate that, in the absence of alternative amplification mechanisms or different physical platforms, direct observation of this effect in free space is unlikely with current or foreseeable experimental capabilities.

ACKNOWLEDGMENTS

We thank Helena Amaral, Thiago Guerreiro, Laura Stolze, and Joanna Zielińska for discussions. This work was partially supported by Conselho Nacional de Desenvolvimento Científico e Tecnológico (CNPq–Brazil), Coordenação de Aperfeiçoamento de Pessoal de Nível Superior (CAPES–Brazil) and Fundação Carlos Chagas Filho de Amparo à Pesquisa do Estado do Rio de Janeiro (FAPERJ–Brazil). JNM acknowledges partial support from a Limitless Space Institute Interstellar Initiative Grant.

Appendix A: Polarizability tensor of a rotating anisotropic particle

This Appendix serves two purposes. First, we provide the details of the derivation leading to the dipole response in Eq. (11). Second, it provides an original expression for the polarizability of a spinning anisotropic particle. To our knowledge, previous results have been limited to rotation about a symmetry axis or to isotropic particles [29].

We consider here an axisymmetric particle rotating about an axis orthogonal to its symmetry direction. This configuration is particularly relevant in view of recent experimental advances [3], where anisotropic dumbbell-like particles have reached record angular frequencies when rotated about an axis perpendicular to their symmetry axis. The present derivation can be extended straightforwardly to more general anisotropic particles without symmetry.

As in the main text, we take a particle with a symmetry along the $\hat{\mathbf{x}}$ direction and rotating about the $\hat{\mathbf{z}}$ axis. \mathcal{R} denotes the laboratory frame and \mathcal{R}' the co-rotating frame where the particle is at rest. In \mathcal{R}' , the dipole response is determined by the standard material response $\boldsymbol{\alpha}_{\text{rest}}(\omega)$ [Eq. (10)] as

$$\mathbf{d}'(\omega) = \boldsymbol{\alpha}_{\text{rest}}(\omega) \cdot \mathbf{E}'(\omega), \quad (\text{A1})$$

The transformation from \mathcal{R}' to \mathcal{R} corresponds to the rotation $\mathbf{r} = \mathcal{R}_z(t)\mathbf{r}'$, with

$$\mathcal{R}_z(t) = \begin{pmatrix} \cos \Omega t & -\sin \Omega t & 0 \\ \sin \Omega t & \cos \Omega t & 0 \\ 0 & 0 & 1 \end{pmatrix}, \quad (\text{A2})$$

Applying this transformation to the electric field relates the lab/co-rotating frame components in the Fourier domain

$$E_x(\omega) \pm iE_y(\omega) = E'_x(\omega \pm \Omega) \pm iE'_y(\omega \pm \Omega), \quad (\text{A3})$$

while the z component remains unchanged. Equation (A3) shows that rotation mixes field components at frequencies shifted by $\pm\Omega$.

Combining (A3) with the dipole relation in the co-rotating frame (A1) and its shifted-frequency counterparts, we obtain (11) for the dipole moment in the laboratory frame with

$$\boldsymbol{\alpha}_0(\omega) = \begin{pmatrix} \frac{1}{2}(S^+ + S^-) & \frac{i}{2}(S^+ - S^-) & 0 \\ -\frac{i}{2}(S^+ - S^-) & \frac{1}{2}(S^+ + S^-) & 0 \\ 0 & 0 & \alpha_{\perp}(\omega) \end{pmatrix}. \quad (\text{A4})$$

We have introduced the polarizability

$$S^{\pm}(\omega) = \frac{\alpha_{\parallel}(\omega \pm \Omega) + \alpha_{\perp}(\omega \pm \Omega)}{2} \quad (\text{A5})$$

taken at the Doppler-shifted frequencies $\omega \pm \Omega$. Eq. (11) shows that the dipole response in the plane orthogonal to the rotation axis at frequency ω is driven by the field modes at shifted frequencies $\omega \pm 2\Omega$.

While our analysis focuses on a spheroidal nanoparticle to simplify the notation, the results extend to more general geometries. For an arbitrary dielectric particle, the polarizability tensor reads $\boldsymbol{\alpha}_{\text{rest}} = \text{diag}(\alpha_1, \alpha_2, \alpha_3)$ when taking the principal axis basis. If the particle rotates about a principal axis (e.g., axis 3 as in Fig. 1), Eqs. (11)–(16) still hold substituting $\alpha_1 - \alpha_2$ for $\Delta = \alpha_{\parallel} - \alpha_{\perp}$. Thus, the frequency modulation at 2Ω survives even for asymmetric particles as long as the rotation axis is not a symmetry axis ($\alpha_1 \neq \alpha_2$). This is a general feature within the dipole approximation and linear regime: because the polarizability α_{ij} is a rank-two tensor, it is inherently invariant under a π -rotation about any axis.

-
- [1] J. Ahn, Z. Xu, J. Bang, Y.-H. Deng, T. M. Hoang, Q. Han, R.-M. Ma, and T. Li, Optically levitated nanodumbbell torsion balance and GHz nanomechanical rotor, *Phys. Rev. Lett.* **121**, 033603 (2018).
 [2] R. Reimann, M. Doderer, E. Hebestreit, R. Diehl, M. Frimmer, D. Windey, F. Tebbenjohanns, and

- L. Novotny, GHz rotation of an optically trapped nanoparticle in vacuum, *Phys. Rev. Lett.* **121**, 033602 (2018).
 [3] J. Ahn, Z. Xu, J. Bang, P. Ju, X. Gao, and T. Li, Ultrasonic torque detection with an optically levitated nanorotor, *Nature Nanotechnology* **15**, 89 (2020).

- [4] Y. Jin, J. Yan, S. J. Rahman, J. Li, X. Yu, and J. Zhang, 6 ghz hyperfast rotation of an optically levitated nanoparticle in vacuum, *Photon. Res.* **9**, 1344 (2021).
- [5] J. A. Zielińska, F. van der Laan, A. Norrman, R. Reimann, M. Frimmer, and L. Novotny, Long-axis spinning of an optically levitated particle: A levitated spinning top, *Phys. Rev. Lett.* **132**, 253601 (2024).
- [6] P. Ju, Y. Jin, K. Shen, Y. Duan, Z. Xu, X. Gao, X. Ni, and T. Li, Near-field GHz rotation and sensing with an optically levitated nanodumbbell, *Nano Letters* **23**, 10157 (2023).
- [7] P. Ju, Y. Jin, K. Shen, Y. Duan, Z. Xu, X. Gao, X. Ni, and T. Li, Near-field GHz rotation and sensing with an optically levitated nanodumbbell, *Nano Letters* **23**, 10157 (2023).
- [8] R. Zhao, A. Manjavacas, F. J. García de Abajo, and J. B. Pendry, Rotational quantum friction, *Phys. Rev. Lett.* **109**, 123604 (2012).
- [9] Z. Xu, Z. Jacob, and T. Li, Enhancement of rotational vacuum friction by surface photon tunneling, *Nanophotonics* **10**, 537 (2021).
- [10] A. Manjavacas and F. J. García de Abajo, Vacuum friction in rotating particles, *Phys. Rev. Lett.* **105**, 113601 (2010).
- [11] M. F. Maghrebi, R. L. Jaffe, and M. Kardar, Spontaneous emission by rotating objects: A scattering approach, *Phys. Rev. Lett.* **108**, 230403 (2012).
- [12] S. Sanders, W. J. M. Kort-Kamp, D. A. R. Dalvit, and A. Manjavacas, Nanoscale transfer of angular momentum mediated by the casimir torque, *Communications Physics* **2**, 71 (2019).
- [13] G. C. Matos, R. Melo e Souza, P. A. Maia Neto, and F. Impens, Quantum vacuum sagnac effect, *Phys. Rev. Lett.* **127**, 270401 (2021).
- [14] H. S. G. Amaral, P. P. Abrantes, F. Impens, P. A. Maia Neto, and R. Melo e Souza, Tailoring the van der waals interaction with rotation, *Phys. Rev. Lett.* **135**, 243601 (2025).
- [15] A. Lambrecht, M.-T. Jaekel, and S. Reynaud, Motion induced radiation from a vibrating cavity, *Phys. Rev. Lett.* **77**, 615 (1996).
- [16] M.-T. Jaekel and S. Reynaud, Movement and fluctuations of the vacuum, *Reports on Progress in Physics* **60**, 863 (1997).
- [17] M. Kardar and R. Golestanian, The “friction” of vacuum, and other fluctuation-induced forces, *Rev. Mod. Phys.* **71**, 1233 (1999).
- [18] M. F. Maghrebi, R. Golestanian, and M. Kardar, Scattering approach to the dynamical Casimir effect, *Phys. Rev. D* **87**, 025016 (2013).
- [19] M. B. Farias, C. D. Fosco, F. C. Lombardo, and F. D. Mazzitelli, Motion induced radiation and quantum friction for a moving atom, *Phys. Rev. D* **100**, 036013 (2019).
- [20] V. Dodonov, Fifty years of the dynamical Casimir effect, *Physics* **2**, 67 (2020).
- [21] T. Gong, M. R. Corrado, A. R. Mahbub, C. Shelden, and J. N. Munday, Recent progress in engineering the Casimir effect, applications to nanophotonics, nanomechanics, and chemistry, *Nanophotonics* **10**, 523 (2021).
- [22] L. M. Woods, M. Krüger, and V. V. Dodonov, Perspective on some recent and future developments in Casimir interactions, *Applied Sciences* **11**, 10.3390/app11010293 (2021).
- [23] F. Impens, R. de Melo e Souza, G. C. Matos, and P. A. Maia Neto, Dynamical Casimir effects with atoms: From the emission of photon pairs to geometric phases, *Europhysics Letters* **138**, 30001 (2022).
- [24] C. M. Wilson, G. Johansson, A. Pourkabirian, M. Simoen, J. R. Johansson, T. Duty, F. Nori, and P. Delsing, Observation of the dynamical Casimir effect in a superconducting circuit, *Nature* **479**, 376 (2011).
- [25] V. Dodonov, A. Klimov, and V. Man’ko, Generation of squeezed states in a resonator with a moving wall, *Physics Letters A* **149**, 225 (1990).
- [26] V. Dodonov and A. Klimov, Long-time asymptotics of a quantized electromagnetic field in a resonator with oscillating boundary, *Physics Letters A* **167**, 309 (1992).
- [27] P. A. Maia Neto and L. A. S. Machado, Quantum radiation generated by a moving mirror in free space, *Physical Review A* **54**, 3420 (1996).
- [28] F. Lombardo and P. Villar, Dynamical Casimir Effect in Superconducting Cavities: From Photon Generation to Universal Quantum Gates, e-print: arXiv 2504.11361 (2025).
- [29] A. Manjavacas and F. G. De Abajo, Thermal and vacuum friction acting on rotating particles, *Physical Review A* **82**, 063827 (2010).
- [30] K. A. Milton, J. S. Hye, and I. Brevik, The reality of Casimir friction, *Symmetry* **8**, 10.3390/sym8050029 (2016).
- [31] D. Reiche, F. Intravaia, and K. Busch, Wading through the void: Exploring quantum friction and nonequilibrium fluctuations, *APL Photonics* **7**, 030902 (2022).
- [32] D. Oue, B. Shapiro, and M. G. Silveirinha, Quantum friction near the instability threshold, *Phys. Rev. B* **111**, 075403 (2025).
- [33] P. H. Pereira, F. Impens, C. Farina, P. A. Maia Neto, and R. de Melo e Souza, Microscopic quantum friction, *Phys. Rev. Lett.* **136**, 193601 (2026).
- [34] A. O. Turkey, M. M. Rashad, A. E.-H. T. Kandil, and M. Bechelany, Tuning the optical, electrical and magnetic properties of $\text{Ba}_{0.5}\text{Sr}_{0.5}\text{Ti}_x\text{M}_{1-x}\text{O}_3$ (BST) nanopowders, *Phys. Chem. Chem. Phys.* **17**, 12553 (2015).
- [35] A. O. Turkey, M. M. Rashad, and M. Bechelany, Tailoring optical and dielectric properties of $\text{Ba}_{0.5}\text{Sr}_{0.5}\text{TiO}_3$ powders synthesized using citrate precursor route, *Materials & Design* **90**, 54 (2016).
- [36] L. H. Ford and A. Vilenkin, Quantum radiation by moving mirrors, *Phys. Rev. D* **25**, 2569 (1982).
- [37] P. A. Maia Neto, Vacuum radiation pressure on moving mirrors, *J. Phys. A: Math. Gen.* **27**, 2167 (1994).
- [38] L. Alonso, G. C. Matos, F. Impens, P. A. Maia Neto, and R. de Melo e Souza, Multipole approach to the dynamical Casimir effect with finite-size scatterers, *Entropy* **26**, 10.3390/e26030251 (2024).
- [39] P. A. Maia Neto and S. Reynaud, Dissipative force on a sphere moving in vacuum, *Phys. Rev. A* **47**, 1639 (1993).
- [40] R. Melo e Souza, F. Impens, and P. A. Maia Neto, Microscopic dynamical Casimir effect, *Phys. Rev. A* **97**, 032514 (2018).
- [41] V. Berestetski, E. M. Lifshitz, and L. Pitaevskii, *Relativistic Quantum Theory Volume 1* (Pergamon, 1971).
- [42] C. Cohen-Tannoudji, J. Dupont-Roc, and G. Grynberg, *Photons and Atoms: Introduction to Quantum Electrodynamics* (Wiley, 1997).
- [43] L. D. Landau and E. M. Lifshits, *Electrodynamics of continuous media* (Pergamon press Oxford, 1946).

- [44] M. Schuck, D. Steinert, T. Nussbaumer, and J. W. Kolar, Ultrafast rotation of magnetically levitated macroscopic steel spheres, *Science Advances* **4**, e1701519 (2018), <https://www.science.org/doi/pdf/10.1126/sciadv.1701519>.